THE JOURNAL OF PHYSICAL CHEMISTRY Letters

Letter

pubs.acs.org/JPCL

Uncovering the Veil of the Degradation in Perovskite $CH_3NH_3PbI_3$ upon Humidity Exposure: A First-Principles Study

Chuan-Jia Tong,[†] Wei Geng,[†] Zhen-Kun Tang,[†] Chi-Yung Yam,[†] Xiao-Li Fan,[‡] Jiang Liu,[§] Woon-Ming Lau,[†,§] and Li-Min Liu*[,†]

[†]Beijing Computational Science Research Center, Beijing 100094, China

[‡]School of Material Science and Engineering, State Key Laboratory of Solidification Processing, Northwestern Polytechnic University, 127 YouYi Western Road, Xi'an, China

[§]Chengdu Green Energy and Green Manufacturing Technology R&D Center, Chengdu, Sichuan 610207, China

ABSTRACT: Methylammonium lead iodide perovskite, $CH_3NH_3PbI_3$ ($MAPbI_3$), has made great progress in its efficiency as used in solid-state solar cells during recent years. Meanwhile, the degradation of its performance in moisture has attracted great attention, but the specific mechanism is not yet fully established. The water effects on the detailed structure and properties of the perovskite $CH_3NH_3PbI_3$ have been carefully explored based on first-principles calculations. The results reveal that the water adsorption energy on the $CH_3NH_3PbI_3$ (001) surface is ~0.30 eV, while the water can easily penetrate into the surface in the form of molecular state owing to the huge interspace of $CH_3NH_3PbI_3$, which can further corrode down the whole structure gradually. More importantly, the deformation of the structure greatly affects the electronic structure, which decreases the optical absorption. Such work paves an important way to understand the initial degradation progress of the perovskite structure under the humidity condition, which should help to optimize the structure to prevent the penetration of water in the system.

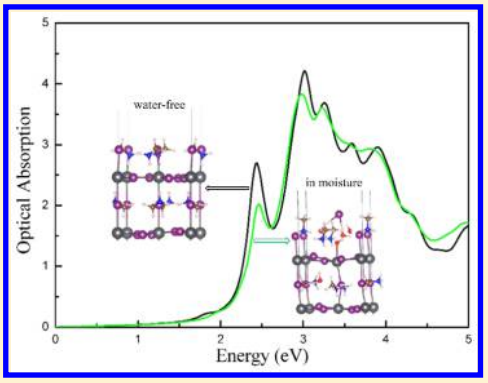

The conversion of solar energy into electricity has attracted great attention because of the increasing energy demands of future generations without negatively impacting the global environment.[1,2] On the contrary, dye-sensitized solar cells (DSCs) based on nanocrystalline metal oxides like TiO_2[3,4] are a promising photovoltaic device for a renewable energy source. In recent years, new organic−inorganic hybrid perovskite compounds ($MAPbX_3$, X = halogen; MA = CH_3NH_3)[5−11] have been used as light harvesters for solid-state DSCs. These $MAPbX_3$ compounds stand out for their low cost, wide light absorption, ferroelectric properties, and high efficiency.[12−18] In fact, since the first reported perovskite solar cell with power conversion efficiency (PCE) of 3.81% by Kojima and coworkers in 2009,[19] the amazing growth rate of PCE about these perovskite materials has been made in the following years. In 2011, Park et al. fabricated $MAPbI_3$ perovskite solar cells with PCE of 6.54%.[20] Then, Kim et al. achieved a PCE of up to 9.7% based on spiro-MeOTAD as hole transport materials in 2012.[21] In 2013, Noh et al. demonstrated highly efficient solar cells of a PCE of 12.3% as a result of tunable composition for $MAPb(I_{1-x}Br_x)_3$.[22] In 2014, Grätzel and coworkers reported an efficiency of 17.01% by controlling the size of $MAPbI_3$ cuboids during their growth.[23] Up to now, the PCE of perovskite-based solar cells reaches nearly 20%.[7]

Although the methylammonium lead iodide $MAPbI_3$ perovskite shows an outstanding performance and tantalizing prospect in solar cells, there are deficiencies needed to overcome at the same time. One vital problem is that $MAPbI_3$ perovskite films are extremely sensitive to moisture in air.[7,8,24−27] Many experiments have demonstrated that the effect of moisture on $MAPbI_3$ plays a crucial role in the performance of perovskite solar cells.[22,28−30] Despite various explanations on the negative influence of H_2O with or without illumination in experiments,[29,30] the intrinsic mechanism is still unknown. It is urgent to understand the intrinsic mechanism on water interaction with the perovskite, especially at the atomic level, to avoid the degradation of efficiency.

In this study, the effect of water molecules on perovskite $MAPbI_3$ was performed by first-principles calculations. A detailed interaction between H_2O and $MAPbI_3$ (001) surface is carefully explored. The results suggest that the water molecules are extremely easy to infiltrate into $MAPbI_3$ surface and then corrode the whole structure step by step. More importantly, during the water corrosion of $MAPbI_3$, a substantial distortion of the structure is observed. Because of the deformation induced by the water, the optical absorption in the visible region is greatly decreased, which should be the main reason for the degradation of the performance of perovskite solar cells. All of these results show a comprehensive picture of the water effects on both the atomic structure and properties of

Received: July 20, 2015
Accepted: August 4, 2015
Published: August 4, 2015

ACS Publications © 2015 American Chemical Society

DOI: 10.1021/acs.jpclett.5b01544
J. Phys. Chem. Lett. 2015, 6, 3289−3295

$MAPbI_3$ upon humidity exposure, and thus the water adsorption and diffusion should be greatly avoided to design the high-performance $MAPbI_3$ in solar cells.

The density functional theory (DFT) calculations were performed using a periodical slab of three-layer thickness $MAPbI_3$ (001) surface with a 40 Å vacuum layer in the z direction. A 2 × 2 supercell including 360 atoms is used. Structural relaxations and ab initio molecular dynamics (AIMD) are performed using CP2K/QUICKSTEP package.[31] The wave functions of the valence electrons were expanded in terms of Gaussian functions with molecularly optimized double-ζ polarized basis sets (m-DZVP), which ensures a small basis set superposition error,[32] and core electrons were described with norm-conserving Goedecker, Teter, and Hutter (GTH) pseudopotentials.[33] The cutoff energy for the hybrid Gaussian plane-wave basis set is as high as 500 Ry to ensure accuracy. Atomic position is fully relaxed until the maximum residual force is <0.01 eV/Å. The exchange correlation energy is calculated with the Perdew−Burke−Ernzerhof (PBE) functional.[34] To improve the description of long-range van der Waals (vdW) interaction, we have employed the DFT-D3(BJ) approach.[35,36]

The AIMD was carried out with the NVT ensemble at a target temperature of 300 K along with a Nosé−Hoover thermostat. The total simulation time is 30 ps with a time step of 1 fs. Additionally, the reaction paths and energy barriers have been carried out with the nudged elastic band (NEB) technique.[37,38] During the NEB calculation, eight images are uniformly distributed along the reaction path connecting the initial and final states.

The corresponding electronic and optical properties were then calculated with the projector augmented wave method, as implemented in VASP,[39−41] along with PBE functional. The cutoff energy of the projector augmented plane-wave basis set is 500 eV to ensure an accuracy of the energy of 1 meV per atom. Electronic minimization was performed with a tolerance of 10^{-5} eV. The k-point sampling uses the Monkhorst−Pack scheme on a 6 × 6 × 1 mesh, and a 40 Å vacuum spacing is maintained to prevent interactions between the adjacent supercells.

Water molecules are put on the three-layer (3L) (001) surface one by one to understand how water interacts with the surface. Here the adsorption energy E_{ads} is defined as

$$E_{ads} = \frac{E_{water/MAPbI3(001)} - N \times E_{water} - E_{MAPbI3(001)}}{N}$$

where $E_{water/MAPbI3(001)}$, E_{water}, and $E_{MAPbI3(001)}$ are the total energies of the total adsorption system, a single water molecule, and the clean $MAPbI_3$ (001) surface, respectively. Here N stands for the number of the adsorbed water molecules.

There exist two typical crystal structures of $MAPbI_3$ perovskite: the tetragonal phase at room temperature and the orthorhombic phase at low temperature (<162 K).[42] $MAPbI_3$ in the tetragonal phase is more stable under the ambient condition,[42] and we only consider the surface of the tetragonal phase in this work. The detailed atomic structures of bulk $MAPbI_3$ are shown in Figure 1a,b. Each Pb atom is coordinated to six I atoms, with four I atoms in the equatorial direction and two I atoms in the apical direction. Four dipolar organic MA^+ ions occupy the interstitial space in the octahedron PbI_6 cage. The optimized lattice constants are found to be a = 8.64, b = 8.67, and c = 12.93 Å, which agree well with previous theoretical and experimental results.[43] As previously reported,[44−46] the (001) surface, which remains the main framework of the bulk material, is one of the most common surfaces of perovskite. In our previous work, the perovskite (001) surface can be either MA^+- or PbI_2-terminated, and the MA^+-terminated one is found to be more stable.[47] In the following, we mainly focus on the water interaction with the MA^+-terminated surface.

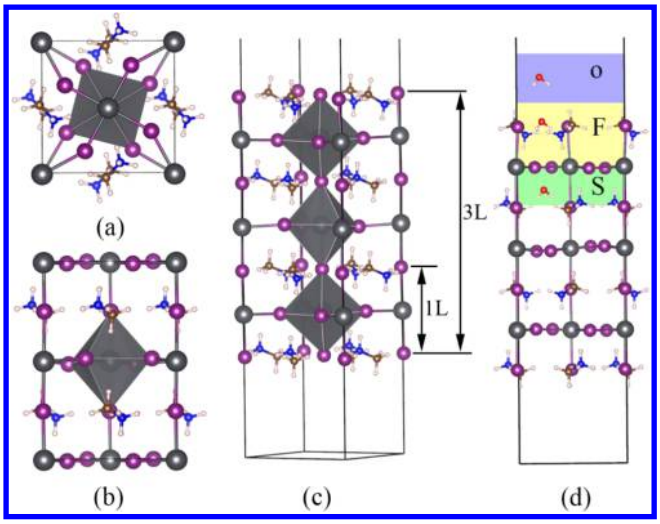

Figure 1. (a) Top and (b) side views of bulk $CH_3NH_3PbI_3$ perovskite. (c) Optimized stable geometrical structures of three-layer slab with (001) surface of $CH_3NH_3PbI_3$ perovskite. (d) Imaginary typical structure of three-layer (001) surface containing water named O1F1S1. The divisional colored regions represent where water molecules possible locate with naming O, F, and S, respectively (dark gray: lead; purple: iodine; brown: carbon; blue: nitrogen; pink: hydrogen).

To easily discuss the possible adsorption position and diffusion process of water molecule on/in the perovskite $MAPbI_3$ in the following, we labeled the upper area of the (001) surface as regions O, F, and S from up to down, respectively. The region O corresponds to water adsorbing on the surface of $MAPbI_3$, and region F (S) represents that water stays in the upper (down) side of the first layer. (See Figure 1d). For simplicity, we label these structures as XN based on the water position and number in the specific region, where X corresponds to the region where water locates and N stands for the number of water molecules in region X. For example, O1F1S1 stands for a $MAPbI_3$ surface with three water molecules, and each of them occupy regions O, F, and S, respectively. The corresponding structure is shown in Figure 1d.

The water adsorption structure on the perovskite $MAPbI_3$ (001) at the low coverage is first explored. One water molecule is put on the $MAPbI_3$ (001) surface. Upon geometry optimization, the water molecule is adsorbed at 2.18 Å above the surface. (See Figure 2.) The adsorption energy of one water molecule is ∼0.30 eV. The interaction between organic molecules MA^+ and water molecule is through the hydrogen bond. To determine the necessary thickness to represent the (001) face of $MAPbI_3$ perovskite, we first examine adsorption energy (E_{ads}) of one H_2O molecule on both 3L and four-layer (4L) slabs of the perovskite $MAPbI_3$ (001). Here we define the thickness of one layer as the height of one octahedron PbI_6 cage, as shown in Figure 1c (the shadow region). The calculated water adsorption energies, E_{ads}, on 3L and 4L are 0.30 and 0.31 eV, respectively, which indicates that the slab

DOI: 10.1021/acs.jpclett.5b01544
J. Phys. Chem. Lett. 2015, 6, 3289−3295

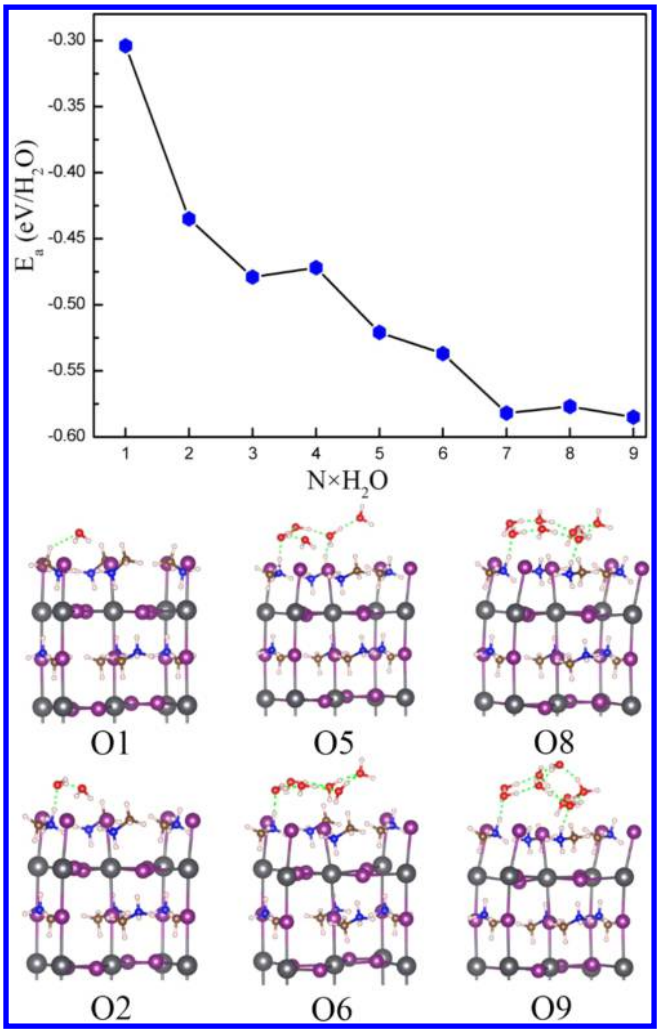

Figure 2. Adsorption energy, E_{ads} (eV/H_2O), of adsorbed system while water molecules stay in region O. The lower part are six typical structures of O1, O2, O5, O6, O8, and O9, respectively. The colored balls represent the different atoms, as shown in Figure 1, and the green dashed line stands for hydrogen bond.

model with a 3L thickness (Figure 1c) is enough to mimic the perovskite $MAPbI_3$ (001) surface.

The corresponding structure O1 is that the water adsorbs above 2.18 Å of the surface (see Figure 2), with the hydrogen atoms pointing down to the iodine atoms. The corresponding distance between the oxygen and the hydrogen atom of MA^+ is ~2.60 Å, which indicates that the interaction between organic molecule MA^+ and water molecule is through the hydrogen bond.

The adsorption energy per water gradually increases from 0.30 to 0.58 eV as the number of adsorbed water molecules increases to 8. During this process, the water molecules prefer to cluster together through hydrogen bonds, and thus the interaction between water also facilitates surface adsorption of water. It should be noted that the maximum number of the water adsorption on the (1 × 1) surface is 8. When the number of water molecules is more than 8, the other water molecules will adsorb above the first layer. Some typical adsorption structures are shown in Figure 2.

To investigate whether water molecules can diffuse from the surface into the subsurface, we examined the related diffusion process for one water molecule moving from region O to the first layer. (See Figure 3a.) Two different kinds of process are considered in this work. The first one is that the water molecule moves from region O into the upper side of first layer (region F). The calculated results are shown in Figure 3a. The water molecule stays in region F and is ~0.18 eV more stable than region O, and thus it is obvious that the water energetically prefers to stay inside (region F) instead of surface (region O). More interesting, the calculated diffusion barrier from the surface to inside region F is only 0.04 eV, and the pretty small value indicates that the water in O1 can easily penetrate into structure F1. The main reason should originate from the special structure of perovskite $MAPbI_3$. Owing to its huge framework consisting of Pb and I atoms, the interstitial space is relatively large, despite the occupation of organic molecules MA^+. Water molecules can thus easily move in without too much resistance. As the water molecule moves inside, the final structure looks quite similar to the initial structure. As shown in Figure 3a, compared with O1, one MA^+ molecule in F1 changes its orientation into the vertical direction (along (001) direction), while the other atoms basically remain unchanged.

Next we consider how the water molecule diffuses further inside the region. The water molecule diffusing from the upper region (region F) to the low region of first layer (region S) is further studied. The calculated diffusion barrier for this process is 0.31 eV, which is a little larger than the one from O1 to F1. While this diffusion barrier is still relatively small, the water molecules should have chance to diffuse from the upper region

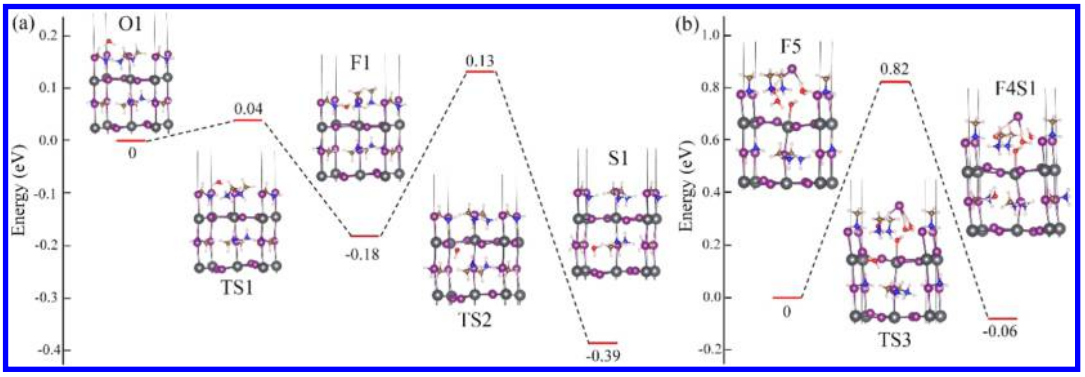

Figure 3. Energy profile of different states in structure transformation: (a) O1 to F1 and F1 to S1 and (b) F5 to F4S1. The inset images are part of the configurations of different states. TS1, TS2, and TS3 stand for the transition states of three different diffusion processes, respectively. Additionally, the energies of structure O1 and F5 are both set to zero.

DOI: 10.1021/acs.jpclett.5b01544
J. Phys. Chem. Lett. 2015, 6, 3289−3295

into the inner one. Meanwhile, the water molecules in region F is ∼0.21 eV more stable than the one in region S. Thus, there is a strong driving force for the water molecule to further diffuse inside of $MAPbI_3$. It should be noted that the diffusion from region F to S is different from region O to F considering that the water molecule needs overcome the distinct frame. The diffusion from O to F needs to overcome the frame of MA^+, and the diffusion from F to S is to overcome the frame of PbI_2. The different diffusion barriers for these two processes should mainly come from these two distinct frames. When the water molecule arrives at the region S, the new appeared structure is the MA^+-terminated (001) surface again. Therefore, the penetration of water can proceed by repeating this process, although the diffusion barrier may have a slight difference from the above one. As the water molecule moves into region S, the original structure, especially the orientation of MA^+ molecule, changes once again, as shown in Figure 3a. First, the changed MA^+ molecule in region F recovers its original orientation, not along the (001) direction any more. Second, one MA^+ molecule in region S with its orientation along (111) in structure F1 now changes its orientation along (010) when converged into structure S1. Such results indicate the water molecule could affect the structure of perovskite $MAPbI_3$.

As previously discussed, the water molecule prefers to diffuse from the surface to the inner region at low coverage. Next, we consider water diffusion from the surface to the inside region at the relative high coverage. To determine in which region the water molecules prefer to stay, the relative energies (E_r) between systems with water molecules staying in regions F and O are calculated

$$E_r(N) = E_F(N) - E_O(N)$$

where E_F and E_O are the total energies of adsorbed system with water molecules stay in region F and O, respectively, and N represents the number of water molecules. The corresponding results are summarized in Figure 4. It is obvious that E_r is negative when the number of water is no more than six ($N \leq 6$). This indicates that water prefers to stay in region F rather than region O.

On the contrary, the degree of deformation for the perovskite $MAPbI_3$ surface increases with increasing N. The deformation here includes the changed site of MA^+ and the distortion of Pb−I bond in region F. In particular, when N becomes four (see Figure 4), a qualitative change appears in surface configuration, where one of the outmost iodine atoms moves ∼2.12 Å away from surface; meanwhile, the oxygen atom of water strongly bonds to the remaining exposed lead atom. As N increases to six, the $MAPbI_3$ structure in region F is entirely destroyed by packed water molecules. The system begins to repel water molecule as the interstitial space is fully occupied. This results in a positive E_r value, which shows that FN ($N > 6$) structures are energetically not stable at high density of water.

As previously discussed, water molecule at the low coverage could further diffuse from the region F to the more inner region with a small energy barrier. It is important to know whether water molecules prefer to diffuse further inside the region at the relative high coverage. To explore this, we consider the typical model of F5, which contains five water molecules in the region F, and we examine how one of the water molecules diffuses from the region F to region S. The calculated energy barrier is ∼0.82 eV. The final configuration of F4S1 is ∼0.06 eV more stable than that of F5, which suggest that water molecule can

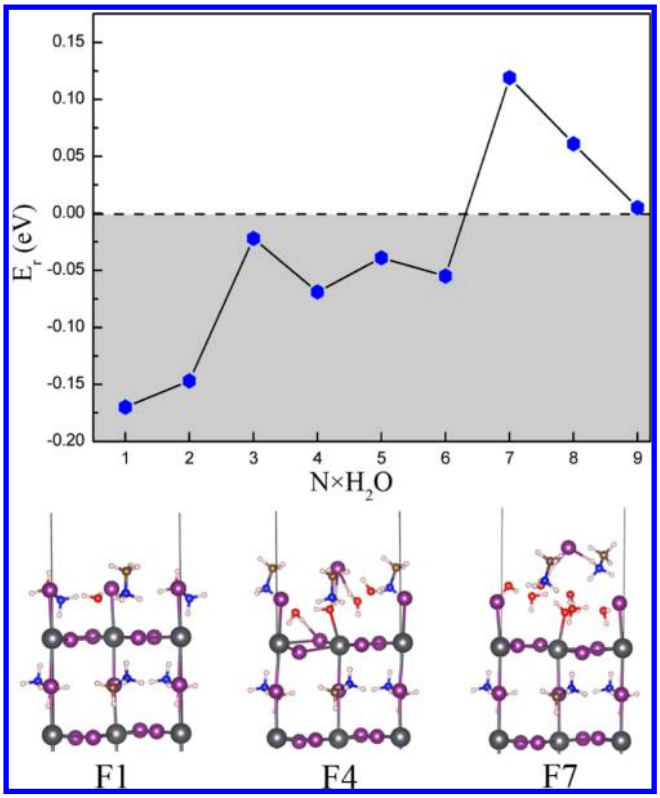

Figure 4. Relative energy, E_r (eV), between structure FN and ON. The value of E_r is negative in the light gray region, which indicates that structure FN is more favorable in energy correspondingly. The lower part shows three typical structures of F1, F4, and F7, respectively.

diffuse from the region F to S at the high coverage of water. In particular, F4S1 induces an additional structural deformation in region S compared with structure F5, as shown in Figure 3b. One of the lead atoms even moves from its original site by ∼0.99 Å, which makes a large distortion of Pb−I bond in region S along with the rotation of the MA^+.

AIMD simulation is further carried out for a water film adsorption on $MAPbI_3$ (001) surface at 300 K to establish the water effect on the $MAPbI_3$ at the finite-temperature. The AIMD simulation is performed with a (2 × 2) supercell. The initial structure contains 24 water molecules at the surface. The AIMD simulation was carried out for 30 ps. Interestingly, 5 of 24 water molecules directly infiltrate into the first layer of slab during the AIMD simulations (See Figure 5a). To show how the water goes from the surface to the inner region, the height of one water molecule is plotted during the simulation. Here the height is defined as the perpendicular distance between its geometric center and the outermost plane form by I atoms. As shown in Figure 5b, the water molecule diffuses from the surface region to the inner region after ∼8 ps; then, the water molecule stays inside for the rest of the simulations, which clearly indicates that water prefers to stay inside of the perovskite $MAPbI_3$. We only see that the water molecules diffuse from the region O to region F during AIMD simulations, and the reason should be the diffusion barrier for the diffusion from region F to S is relative large, as previously discussed.

As previously shown, the perovskite $MAPbI_3$ surface experiences a large deformation after water diffusing from the surface to the inner region. It is natural to ask whether the water molecules will change the electronic structures of

DOI: 10.1021/acs.jpclett.5b01544
J. Phys. Chem. Lett. 2015, 6, 3289−3295

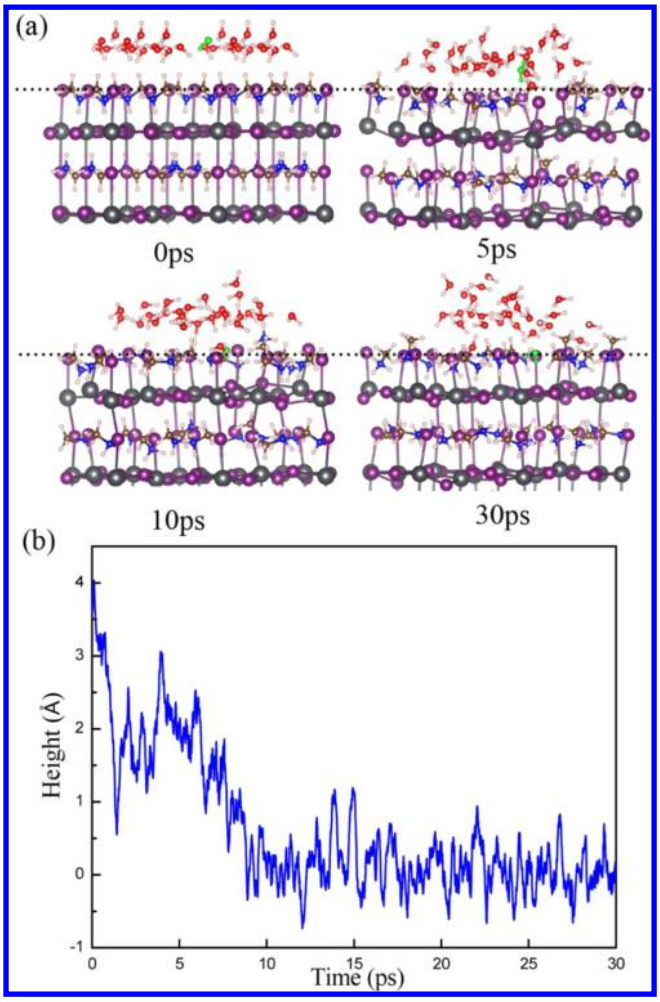

Figure 5. (a) Part of the (2 × 2) supercell containing 24 water molecules after 0, 5, 10, and 30 ps molecular dynamics simulations, respectively. The green water molecule is one of the penetrated water after MD simulation, and the black dotted line stands for the horizontal plane where the outermost I atoms locate in vertical direction at 0 ps. (b) Height between the geometric center of green water molecule and the black dotted line during the MD simulation.

perovskite $MAPbI_3$. Then, the density of states (DOS) of both systems with or without water is calculated, and the results are shown in Figure 6. Here four typical systems are examined: the clean one (3L (001) surface), the one with water adsorption at the region O (O5), and the other two with water staying at inner region (F5 and F4S1).

First of all, we concentrate on the DOS of the clean one, which shows a band gap of ∼1.58 eV. When water adsorbs on the surface, the electronic structure does not change except for a slightly upshift (to 1.62 eV) of the conduction band minimum (CBM) because water only interacts with the surface through hydrogen bond. When water further diffuses into the inner structure, there is a substantial change in electronic structures of both structure F5 and F4S1. The corroded structure in region F no longer dominates the CBM; instead, it contributes to the slightly higher energy level than CBM. In particular, CBM of structure F4S1 is greatly up-shifted compared with the clean one, while its valence band maximum (VBM) does not change, and thus the band gap of the deformed structure F4S1 increases to 1.74 eV, which is ∼0.2 eV larger than the one of clean one.

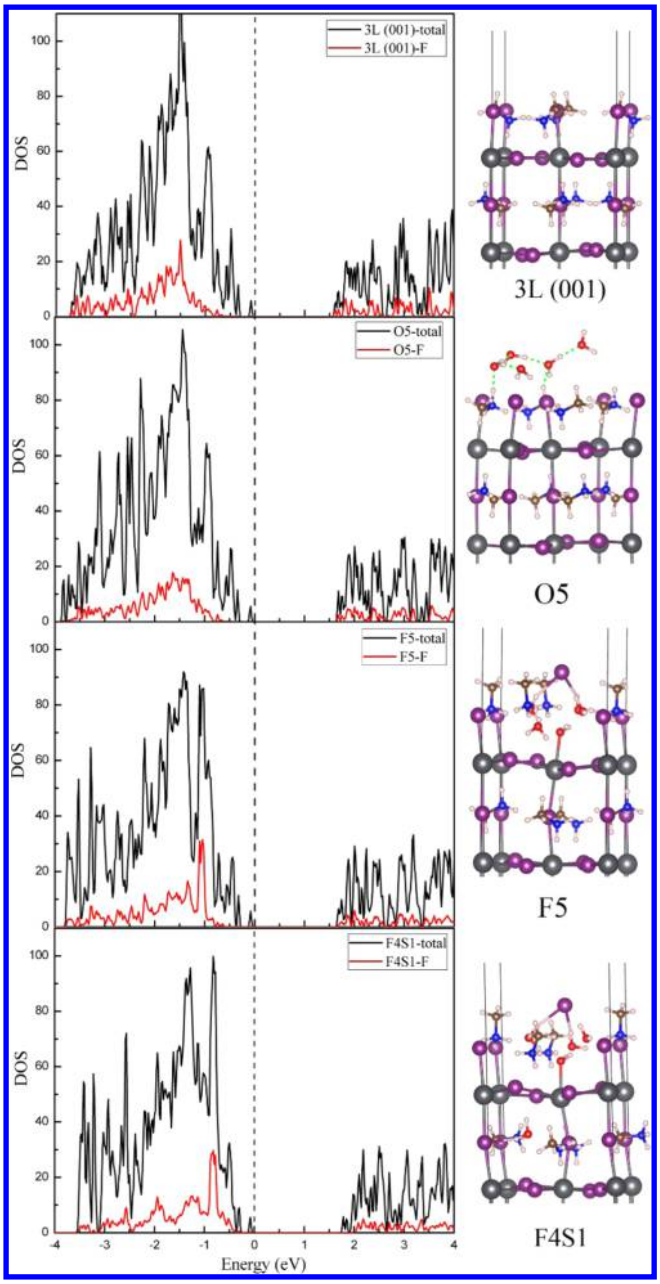

Figure 6. Calculated density of states and corresponding optimized configurations for the four different typical structures: the clean one (3L (001) surface), the one with water adsorption at the region O (O5), and the other two with water staying at inner region (F5 and F4S1). The black dashed line stands for the Fermi level. The thick black and red curves represent the total DOS of all atoms and the DOS of atoms only in region F, correspondingly.

From all of the above, the penetration of water molecules greatly affects not only the configuration but also electronic structures. Moreover, the corroded structure tends to show a larger band gap, which corresponds well with that the structure distortion, and Pb−I bond breaking can lead to an increased band gap.[48] Because the reasonable band gap of perovskite $MAPbI_3$ is critical for its wide light absorption, the relative larger band gap of the water-embedded $MAPbI_3$ may be one reason for the decreasing of its PCE.

It is well known that the high PCE of perovskite is mainly attributed to the strong absorption in the visible-light region so that the photoactive material can effectively utilize solar

DOI: 10.1021/acs.jpclett.5b01544
J. Phys. Chem. Lett. 2015, 6, 3289−3295

energy.[49−51] It is essential to know whether the water molecules will also affect the optical properties of the previously mentioned materials. The same four typical systems, the clean one (3L (001) surface), the one with water adsorption at the region O (O5), and the other two with water staying at inner region (F5 and F4S1), are considered. The calculated optical spectrum for the different structures is shown in Figure 7.

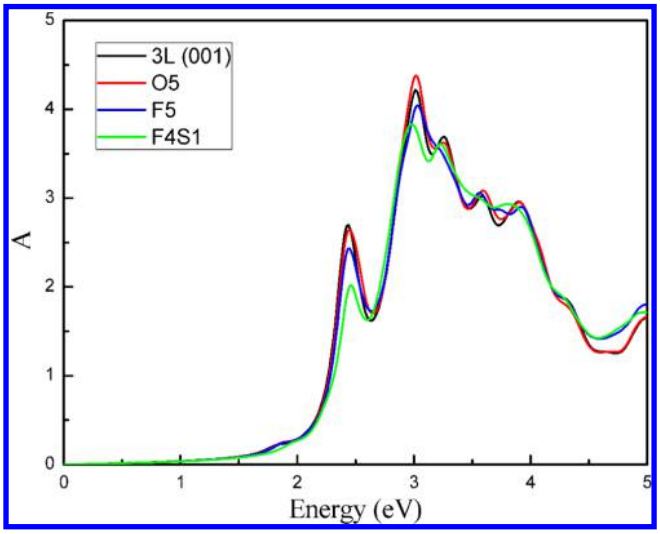

Figure 7. Calculated optical absorbance spectrum $A(\omega)$ of four different typical structures using PBE functional.

The clean $MAPbI_3$ has a very strong intensity in a range of ω from 2.3 to 2.7 eV, which is in the visible-light region, and the maximum value is at ω = ~2.5 eV. When water molecules adsorb on the surface of $MAPbI_3$, the calculated intensity of O5 is quite close to the one of the clean $MAPbI_3$, and the reason should be that the interaction between the water and $MAPbI_3$ is rather weak, and the structure does not change obviously after water adsorbs. When the water molecules diffuse from the surface to the inner region (structure F5), the corresponding intensity around 2.5 eV decreases ~10.4% because water molecules begin to destroy the perovskite structure in region F. When one water molecule of F5 further diffuses from the region F to S, the intensity of the optical absorption of F4S1 further decreases by ~25.9% compared with that of the clean one. It should be noted that the corresponding structure experiences a more serious deformation in region S. (See Figure 6.) In other words, the degree of degradation of the optical absorption is greatly affected by the degree of structure deformation.

In summary, to understand the specific mechanism of PCE degradation upon humidity exposure in perovskite $MAPbI_3$, we investigate the interaction between water molecules and (001) surface of $MAPbI_3$ by first-principles calculations. The calculated results indicate that water can easily penetrate from the surface into the inner region owing to the large interspace in the special perovskite $MAPbI_3$ structure. The penetration of water into the inner region induces structure deformation of the $MAPbI_3$, which greatly decreases the stability of the corresponding regions depending on the number of the water molecules. More importantly, the deformation induced by water greatly affects the electronic properties, which decreases the intensity of optical absorption because of the enlargement of the band gap. These results clarify that degradation of the performance of perovskite solar cells originates from the structure deformation inducing by penetrating of water molecules, which not only helps to understand the corresponding experimental results but also provides the idea to avoid this degradation at the atomic level.

AUTHOR INFORMATION

Corresponding Author

*E-mail: limin.liu@csrc.ac.cn.

Notes

The authors declare no competing financial interest.

ACKNOWLEDGMENTS

This work was supported by the National Natural Science Foundation of China (No. 51222212, 11447011), the MOST of China (973 Project, Grant No. 2011CB922200), and the Science and Technology Development Foundation of China Academy of Engineering Physics (2014A0302015 and 2014B0302054).

REFERENCES

(1) Raga, S. R.; Barea, E. M.; Fabregat-Santiago, F. Analysis of the Origin of Open Circuit Voltage in Dye Solar Cells. *J. Phys. Chem. Lett.* **2012**, *3* (12), 1629−1634.

(2) Gratzel, M. Photoelectrochemical cells. *Nature* **2001**, *414* (6861), 338−344.

(3) Li, Y.-F.; Liu, Z.-P. Particle Size, Shape and Activity for Photocatalysis on Titania Anatase Nanoparticles in Aqueous Surroundings. *J. Am. Chem. Soc.* **2011**, *133* (39), 15743−15752.

(4) Liu, L.-M.; Li, S.-C.; Cheng, H.; Diebold, U.; Selloni, A. Growth and Organization of an Organic Molecular Monolayer on TiO2: Catechol on Anatase (101). *J. Am. Chem. Soc.* **2011**, *133* (20), 7816−7823.

(5) Grinberg, I.; West, D. V.; Torres, M.; Gou, G.; Stein, D. M.; Wu, L.; Chen, G.; Gallo, E. M.; Akbashev, A. R.; Davies, P. K.; Spanier, J. E.; Rappe, A. M. Perovskite oxides for visible-light-absorbing ferroelectric and photovoltaic materials. *Nature* **2013**, *503* (7477), 509−512.

(6) Raga, S. R.; Jung, M.-C.; Lee, M. V.; Leyden, M. R.; Kato, Y.; Qi, Y. Influence of Air Annealing on High Efficiency Planar Structure Perovskite Solar Cells. *Chem. Mater.* **2015**, *27* (5), 1597−1603.

(7) Zhou, H.; Chen, Q.; Li, G.; Luo, S.; Song, T.-b.; Duan, H.-S.; Hong, Z.; You, J.; Liu, Y.; Yang, Y. Interface engineering of highly efficient perovskite solar cells. *Science* **2014**, *345* (6196), 542−546.

(8) Habisreutinger, S. N.; Leijtens, T.; Eperon, G. E.; Stranks, S. D.; Nicholas, R. J.; Snaith, H. J. Carbon Nanotube/Polymer Composites as a Highly Stable Hole Collection Layer in Perovskite Solar Cells. *Nano Lett.* **2014**, *14* (10), 5561−5568.

(9) Lee, M. M.; Teuscher, J.; Miyasaka, T.; Murakami, T. N.; Snaith, H. J. Efficient Hybrid Solar Cells Based on Meso-Superstructured Organometal Halide Perovskites. *Science* **2012**, *338* (6107), 643−647.

(10) Stroppa, A.; Quarti, C.; De Angelis, F.; Picozzi, S. Ferroelectric Polarization of CH3NH3PbI3: A Detailed Study Based on Density Functional Theory and Symmetry Mode Analysis. *J. Phys. Chem. Lett.* **2015**, *6* (12), 2223−2231.

(11) Agiorgousis, M. L.; Sun, Y.-Y.; Zeng, H.; Zhang, S. Strong Covalency-Induced Recombination Centers in Perovskite Solar Cell Material CH3NH3PbI3. *J. Am. Chem. Soc.* **2014**, *136* (41), 14570−14575.

(12) Park, N.-G. Organometal Perovskite Light Absorbers Toward a 20% Efficiency Low-Cost Solid-State Mesoscopic Solar Cell. *J. Phys. Chem. Lett.* **2013**, *4* (15), 2423−2429.

(13) Hao, F.; Stoumpos, C. C.; Chang, R. P. H.; Kanatzidis, M. G. Anomalous Band Gap Behavior in Mixed Sn and Pb Perovskites Enables Broadening of Absorption Spectrum in Solar Cells. *J. Am. Chem. Soc.* **2014**, *136* (22), 8094−8099.

DOI: 10.1021/acs.jpclett.5b01544
J. Phys. Chem. Lett. 2015, 6, 3289−3295

(14) Yun, J. S.; Ho-Baillie, A.; Huang, S.; Woo, S. H.; Heo, Y.; Seidel, J.; Huang, F.; Cheng, Y.-B.; Green, M. A. Benefit of Grain Boundaries in Organic−Inorganic Halide Planar Perovskite Solar Cells. *J. Phys. Chem. Lett.* **2015**, *6* (5), 875−880.
(15) Fan, Z.; Xiao, J.; Sun, K.; Chen, L.; Hu, Y.; Ouyang, J.; Ong, K. P.; Zeng, K.; Wang, J. Ferroelectricity of CH3NH3PbI3 Perovskite. *J. Phys. Chem. Lett.* **2015**, *6*, 1155−1161.
(16) Roldan-Carmona, C.; Malinkiewicz, O.; Betancur, R.; Longo, G.; Momblona, C.; Jaramillo, F.; Camacho, L.; Bolink, H. J. High efficiency single-junction semitransparent perovskite solar cells. *Energy Environ. Sci.* **2014**, *7*, 2968−2973.
(17) Ma, J.; Wang, L.-W. Nanoscale Charge Localization Induced by Random Orientations of Organic Molecules in Hybrid Perovskite CH3NH3PbI3. *Nano Lett.* **2015**, *15* (1), 248−253.
(18) Stroppa, A.; Di Sante, D.; Barone, P.; Bokdam, M.; Kresse, G.; Franchini, C.; Whangbo, M.-H.; Picozzi, S. Tunable ferroelectric polarization and its interplay with spin−orbit coupling in tin iodide perovskites. *Nat. Commun.* **2014**, *5*, 5900.
(19) Kojima, A.; Teshima, K.; Shirai, Y.; Miyasaka, T. Organometal Halide Perovskites as Visible-Light Sensitizers for Photovoltaic Cells. *J. Am. Chem. Soc.* **2009**, *131* (17), 6050−6051.
(20) Im, J.-H.; Lee, C.-R.; Lee, J.-W.; Park, S.-W.; Park, N.-G. 6.5% efficient perovskite quantum-dot-sensitized solar cell. *Nanoscale* **2011**, *3* (10), 4088−4093.
(21) Kim, H.-S.; Lee, C.-R.; Im, J.-H.; Lee, K.-B.; Moehl, T.; Marchioro, A.; Moon, S.-J.; Humphry-Baker, R.; Yum, J.-H.; Moser, J. E.; Gratzel, M.; Park, N.-G. Lead Iodide Perovskite Sensitized All-Solid-State Submicron Thin Film Mesoscopic Solar Cell with Efficiency Exceeding 9%. *Sci. Rep.* **2012**, *2*, 591.
(22) Noh, J. H.; Im, S. H.; Heo, J. H.; Mandal, T. N.; Seok, S. I. Chemical Management for Colorful, Efficient, and Stable Inorganic−Organic Hybrid Nanostructured Solar Cells. *Nano Lett.* **2013**, *13* (4), 1764−1769.
(23) Im, J.-H.; Jang, I.-H.; Pellet, N.; Grätzel, M.; Park, N.-G. Growth of CH3NH3PbI3 cuboids with controlled size for high-efficiency perovskite solar cells. *Nat. Nanotechnol.* **2014**, *9* (11), 927−932.
(24) Burschka, J.; Pellet, N.; Moon, S. J.; Humphry-Baker, R.; Gao, P.; Nazeeruddin, M. K.; Gratzel, M. Sequential deposition as a route to high-performance perovskite-sensitized solar cells. *Nature* **2013**, *499* (7458), 316−319.
(25) Bass, K. K.; McAnally, R. E.; Zhou, S.; Djurovich, P. I.; Thompson, M. E.; Melot, B. C. Influence of moisture on the preparation, crystal structure, and photophysical properties of organohalide perovskites. *Chem. Commun. (Cambridge, U. K.)* **2014**, *50* (99), 15819−15822.
(26) Smith, I. C.; Hoke, E. T.; Solis-Ibarra, D.; McGehee, M. D.; Karunadasa, H. I. A Layered Hybrid Perovskite Solar-Cell Absorber with Enhanced Moisture Stability. *Angew. Chem.* **2014**, *126* (42), 11414−11417.
(27) Cheng, Z.; Lin, J. Layered organic-inorganic hybrid perovskites: structure, optical properties, film preparation, patterning and templating engineering. *CrystEngComm* **2010**, *12* (10), 2646−2662.
(28) Leijtens, T.; Eperon, G. E.; Pathak, S.; Abate, A.; Lee, M. M.; Snaith, H. J. Overcoming ultraviolet light instability of sensitized TiO2 with meso-superstructured organometal tri-halide perovskite solar cells. *Nat. Commun.* **2013**, *4*, 2885.
(29) Niu, G.; Li, W.; Meng, F.; Wang, L.; Dong, H.; Qiu, Y. Study on the stability of CH3NH3PbI3 films and the effect of post-modification by aluminum oxide in all-solid-state hybrid solar cells. *J. Mater. Chem. A* **2014**, *2* (3), 705−710.
(30) Christians, J. A.; Miranda Herrera, P. A.; Kamat, P. V. Transformation of the Excited State and Photovoltaic Efficiency of CH3NH3PbI3 Perovskite upon Controlled Exposure to Humidified Air. *J. Am. Chem. Soc.* **2015**, *137* (4), 1530−1538.
(31) VandeVondele, J.; Krack, M.; Mohamed, F.; Parrinello, M.; Chassaing, T.; Hutter, J. Quickstep: Fast and accurate density functional calculations using a mixed Gaussian and plane waves approach. *Comput. Phys. Commun.* **2005**, *167* (2), 103−128.
(32) VandeVondele, J.; Hutter, J. Gaussian basis sets for accurate calculations on molecular systems in gas and condensed phases. *J. Chem. Phys.* **2007**, *127* (11), 114105.
(33) Goedecker, S.; Teter, M.; Hutter, J. Separable dual-space Gaussian pseudopotentials. *Phys. Rev. B: Condens. Matter Mater. Phys.* **1996**, *54* (3), 1703−1710.
(34) Perdew, J. P.; Burke, K.; Ernzerhof, M. Generalized Gradient Approximation Made Simple. *Phys. Rev. Lett.* **1996**, *77*, 3865−3868.
(35) Grimme, S.; Antony, J.; Ehrlich, S.; Krieg, H. A consistent and accurate ab initio parametrization of density functional dispersion correction (DFT-D) for the 94 elements H-Pu. *J. Chem. Phys.* **2010**, *132* (15), 154104.
(36) Grimme, S.; Ehrlich, S.; Goerigk, L. Effect of the damping function in dispersion corrected density functional theory. *J. Comput. Chem.* **2011**, *32* (7), 1456−1465.
(37) Henkelman, G.; Uberuaga, B. P.; Jónsson, H. A climbing image nudged elastic band method for finding saddle points and minimum energy paths. *J. Chem. Phys.* **2000**, *113* (22), 9901−9904.
(38) Henkelman, G.; Jónsson, H. Improved tangent estimate in the nudged elastic band method for finding minimum energy paths and saddle points. *J. Chem. Phys.* **2000**, *113* (22), 9978−9985.
(39) Kresse, G.; Furthmüller, J. Efficient iterative schemes for ab initio total-energy calculations using a plane-wave basis set. *Phys. Rev. B: Condens. Matter Mater. Phys.* **1996**, *54*, 11169−11186.
(40) Blochl, P. E. Projector augmented-wave method. *Phys. Rev. B: Condens. Matter Mater. Phys.* **1994**, *50*, 17953−17979.
(41) Kresse, G.; Joubert, D. From ultrasoft pseudopotentials to the projector augmented-wave method. *Phys. Rev. B: Condens. Matter Mater. Phys.* **1999**, *59*, 1758−1775.
(42) Kawamura, Y.; Mashiyama, H.; Hasebe, K. Structural Study on Cubic−Tetragonal Transition of CH3NH3PbI3. *J. Phys. Soc. Jpn.* **2002**, *71* (7), 1694−1697.
(43) Baikie, T.; Fang, Y.; Kadro, J. M.; Schreyer, M.; Wei, F.; Mhaisalkar, S. G.; Graetzel, M.; White, T. J. Synthesis and crystal chemistry of the hybrid perovskite (CH3NH3)PbI3 for solid-state sensitised solar cell applications. *J. Mater. Chem. A* **2013**, *1* (18), 5628−5641.
(44) Zhang, H.; Huang, H.; Haule, K.; Vanderbilt, D. Quantum anomalous Hall phase in (001) double-perovskite monolayers via intersite spin-orbit coupling. *Phys. Rev. B: Condens. Matter Mater. Phys.* **2014**, *90* (16), 165143.
(45) Suthirakun, S.; Ammal, S. C.; Muñoz-García, A. B.; Xiao, G.; Chen, F.; zur Loye, H.-C.; Carter, E. A.; Heyden, A. Theoretical Investigation of H2 Oxidation on the Sr2Fe1.5Mo0.5O6 (001) Perovskite Surface under Anodic Solid Oxide Fuel Cell Conditions. *J. Am. Chem. Soc.* **2014**, *136* (23), 8374−8386.
(46) Piskunov, S.; Kotomin, E. A.; Heifets, E.; Maier, J.; Eglitis, R. I.; Borstel, G. Hybrid DFT calculations of the atomic and electronic structure for ABO3 perovskite (0 0 1) surfaces. *Surf. Sci.* **2005**, *575* (1−2), 75−88.
(47) Geng, W.; Zhang, L.; Zhang, Y.-N.; Lau, W.-M.; Liu, L.-M. First-Principles Study of Lead Iodide Perovskite Tetragonal and Orthorhombic Phases for Photovoltaics. *J. Phys. Chem. C* **2014**, *118* (34), 19565−19571.
(48) Yin, W.-J.; Shi, T.; Yan, Y. Unique Properties of Halide Perovskites as Possible Origins of the Superior Solar Cell Performance. *Adv. Mater.* **2014**, *26* (27), 4653−4658.
(49) Zhang, H.; Tong, C.-J.; Zhang, Y.; Zhang, Y.-N.; Liu, L.-M. Porous BN for hydrogen generation and storage. *J. Mater. Chem. A* **2015**, *3*, 9632−9637.
(50) Maggio, E.; Martsinovich, N.; Troisi, A. Evaluating Charge Recombination Rate in Dye-Sensitized Solar Cells from Electronic Structure Calculations. *J. Phys. Chem. C* **2012**, *116* (14), 7638−7649.
(51) Fujishima, A.; Zhang, X.; Tryk, D. A. TiO2 photocatalysis and related surface phenomena. *Surf. Sci. Rep.* **2008**, *63* (12), 515−582.

DOI: 10.1021/acs.jpclett.5b01544
J. Phys. Chem. Lett. 2015, 6, 3289−3295